

Self-organization of antiperiodic oscillations

J.G. Freire^{1,2}, C. Cabeza³, A.C. Marti^{2,3}, T. Pöschel^{1,2}, and J.A.C. Gallas^{1,2,3,4,5,a}

¹ Institute for Multiscale Simulations, Friedrich-Alexander-Universität, 91052 Erlangen, Germany

² Departamento de Física, Universidade Federal da Paraíba, 58051-970 João Pessoa, Brazil

³ Instituto de Física, Facultad de Ciencias, Universidad de la República, Iguá 4225, Montevideo, Uruguay

⁴ Instituto de Altos Estudos da Paraíba, Rua Infante Dom Henrique 100–1801, 58039-150 João Pessoa, Brazil

⁵ Department of Mathematics, Imperial College London, 180 Queen's Gate, London SW7 2AZ, UK

Received 25 May 2014 / Received in final form 17 October 2014

Published online 10 December 2014

Abstract. *Antiperiodic* oscillations forming infinite cascades of spirals were recently found experimentally and numerically in the control parameter space of an autonomous electronic circuit. They were discovered while recording one specific voltage of the circuit. Here, we show that such regular self-organization may be measured in any of the four variables of the circuit. Although the relative size of individual phases, their boundaries and the number of peaks of each characteristic oscillation depends on the physical quantity used to record them, the global structural organization of the complex phase diagrams is an invariant of the circuit. Tunable families of antiperiodic oscillations cast fresh light on new intricate behavior of nonlinear systems and open the possibility of studying hitherto unobserved phenomena.

1 Introduction

The study of regular patterns in the control *parameter space* of nonlinear systems of all sorts is a topic attracting increasing attention in several scientific disciplines in recent years [1–33]. One amazing class of regular patterns, certain spiral-shaped stability phases, arises from the self-organization of *antiperiodic* oscillations, namely from oscillations $x(t)$ that obey the relation $x(t + T) = -x(t)$ for all t , where T is called the antiperiod of $x(t)$. Trivial examples are the trigonometric $x(t) = \sin t$ and $\cos t$ functions. Recently, infinite hierarchies of antiperiodic oscillations displaying waveforms with an ever increasing complexity were found experimentally and numerically to be generated profusely by a certain electronic circuit (Fig. 1) governed by four independent variables [6, 7]. Although antiperiodic oscillations were detected in all four variables of the circuit, all spirals reported earlier were determined for

^a e-mail: jason.gallas@cbi.uni-erlangen.de

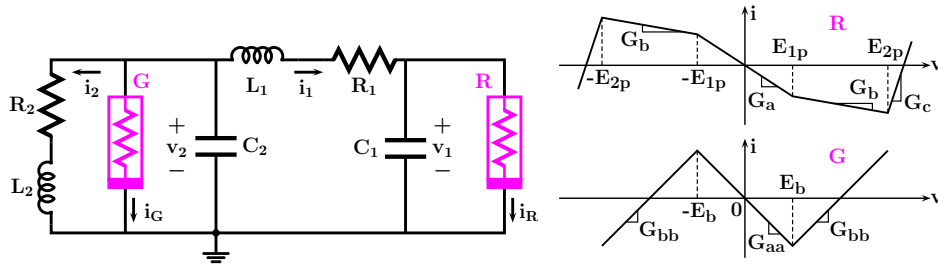


Fig. 1. Schematic representation of the autonomous circuit which generates antiperiodic oscillations. The right column gives the v - i characteristic functions $i_R(v_1)$ and $i_G(v_2)$ of the nonlinear elements. Top: the $v \times i$ characteristic of the nonlinear resistor R . Bottom: the $v \times i$ characteristic of the negative conductance G . Both characteristics are defined by odd-symmetric functions.

just one of the variables [6, 7]. Therefore, it is natural to inquire whether or not the regularities found for one of the variables are also borne out for any arbitrary dynamical variable of the circuit. This is the *Leitmotiv* of the present work.

Our present aim is to report extensive numerical calculations for all four variables of the circuit. We show that the relative size of individual stability phases, their boundaries, and the number of peaks of their characteristic oscillations depends on the physical quantity used to record them. However, despite the differences mentioned, the global structural organization of the complex phase diagrams remains remarkably invariant to these features. Before proceeding, it is perhaps important to mention that there is no analytical method capable of anticipating size and shape of stability phases arising from complex oscillations which can only be found numerically. We find the complexification of all currents and voltages to be mediated by an apparently infinite sequence of antiperiodic oscillations which emerge organized in regular spiral phases in the control parameter space.

The next Section describes the circuit used. Section 3 presents our main findings, namely how the set of stable oscillations gets self-organized as function of control parameters. Section 4 summarizes our findings.

2 The autonomous electronic circuit

The circuit investigated here is shown in Fig. 1. Briefly, it is an autonomous circuit with two active elements, a nonlinear resistor R and a negative conductance G . The characteristic v - i response curves of the active elements are piecewise-linear odd-symmetric functions also shown in Fig. 1. The circuit is governed by the equations:

$$\begin{aligned}
 C_1 \frac{dv_1}{dt} &= i_1 - i_R(v_1), & C_2 \frac{dv_2}{dt} &= -i_1 - i_2 - i_G(v_2), \\
 L_1 \frac{di_1}{dt} &= v_2 - v_1 - i_1 R_1, & L_2 \frac{di_2}{dt} &= v_2 - i_2 R_2,
 \end{aligned} \tag{1}$$

where v_1 (resp. v_2) represent the voltage across the capacitance C_1 (C_2) and i_1 (i_2) is the current through the inductance L_1 (L_2).

Table 1. Reference parameters used in the simulations.

$L_1 = 9.8 \text{ mH}$	$E_{1p} = 2.5 \text{ V}$	$G_a = -0.7 \text{ mS}$
$L_2 = 20.6 \text{ mH}$	$E_{2p} = 11.0 \text{ V}$	$G_b = -0.5 \text{ mS}$
$C_1 = 6 \text{ nF}$	$E_b = 7.5 \text{ V}$	$G_{aa} = -0.5 \text{ mS}$
$C_2 = 12 \text{ nF}$	$G_c = 3.35 \text{ mS}$	$G_{bb} = 0.5 \text{ mS}$

The v - i characteristics of the nonlinear elements are represented by the following odd-symmetric expressions

$$i_R(v_1) = G_c v_1 + (G_a - G_b)(|v_1 + E_{1p}| - |v_1 - E_{1p}|)/2 + (G_b - G_c)(|v_1 + E_{2p}| - |v_1 - E_{2p}|)/2, \quad (2)$$

$$i_G(v_2) = G_{bb} v_2 + (G_{aa} - G_{bb})(|v_2 + E_b| - |v_2 - E_b|)/2. \quad (3)$$

The different parameters are functions of the electronic components. Thus, E_b depends of the output voltage swing, V_{sat} , of the operational amplifier, and of its input voltage, V_{cc} . The slopes G_a and G_b of R depend of the non-zero forward voltage, V_γ , of the diodes which we model as an ideal diode plus a battery. Unless otherwise stated, the values of the several reactances used are the ones summarized in Table 1. Our main goal here is to report details about the unfolding of cascades of antiperiodic patterns discovered in the circuit.

3 Stability diagrams

To locate promising parameter windows to perform experiments, we first computed detailed stability diagrams for our circuit. To this end, Eqs. (1) were integrated systematically over grids of equally spaced parameters using a standard Runge-Kutta fourth-order algorithm with fixed time step $h = 10^{-6}$ s. Such high-resolution computations are quite demanding and were performed on a Altix cluster of 1536 high-performance processors running during a period of several weeks. Computations were started always from a fixed initial condition $v_1 = 8 \text{ V}$, $v_2 = -5 \text{ V}$, $i_1 = -1 \text{ mA}$, $i_2 = 3 \text{ mA}$. The first $\tau \simeq 20 \times 10^5$ integration steps were discarded as transient and the subsequent $20 \times \tau$ steps were used to calculate the Lyapunov spectrum. As it is known, positive exponents indicate chaotic oscillations while a negative largest exponent is a signature of periodic oscillations. The chaotic or periodic nature of solutions was also determined in an independent way, by computing the so-called *isospike diagrams*, diagrams recording the number of peaks (local maxima) within one period of the oscillations. Such diagrams proved useful in recent investigations of models of excitable systems [20] and mixed-mode oscillations [21]. To produce them, subsequently to the computation of the Lyapunov spectrum, numerical integration was continued for an additional $20 \times \tau$ time-steps during which we recorded extrema (maxima and minima) of a given variable of interest together with the instant when they occur. For each time-series we recorded up to 800 extrema, checking whether pulses repeated or not and counting the number of peaks within one period of the periodic oscillations.

Over wide parameter ranges, Fig. 2 presents stability diagrams which discriminate the chaotic or periodic nature of the oscillations in the $R_2 \times R_1$ parameter. This figure shows isospike diagrams [20,21] illustrating in colors the distribution of the number of peaks present in one period of v_2 . As indicated by the colorbar, we use a palette with 17 colors to represent the number of peaks found in one period of the periodic oscillations. Oscillations containing a higher number of peaks are plotted “recycling” these 17 basic colors modulo 17, namely by assigning to higher periods the color-index

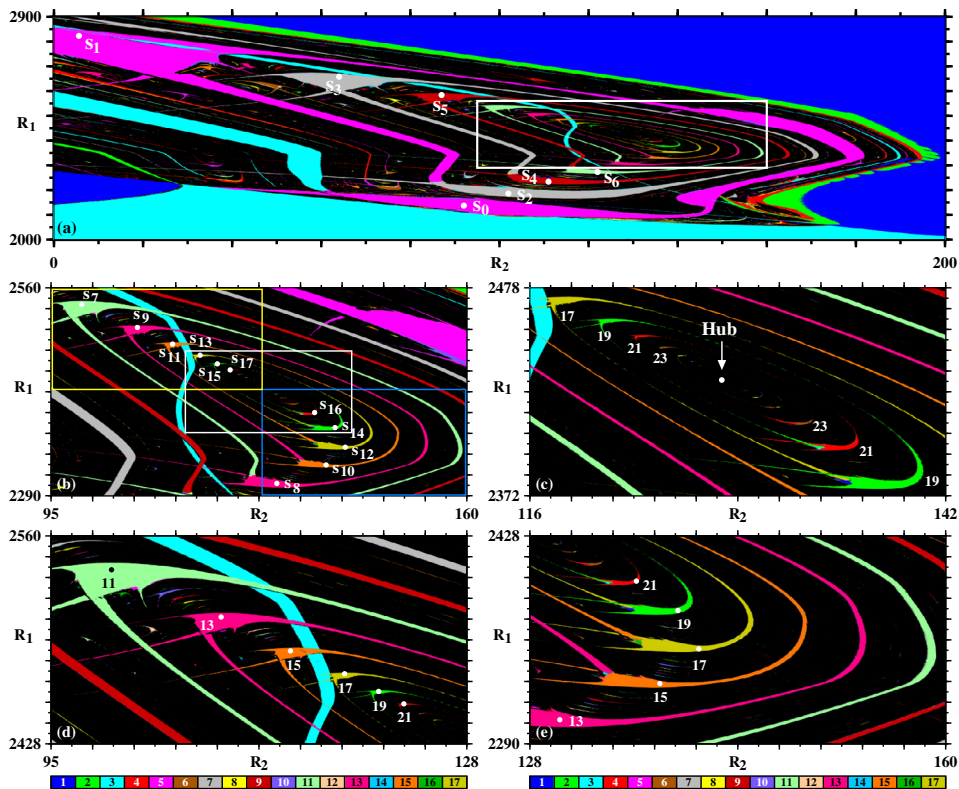


Fig. 2. (a) Global view of a spiral cascade formed by antiperiodic oscillations. (b) Details of the regular organization near the focal point. The focal hub is located inside the white box, where the yellow and blue boxes meet. (c) Magnification around the focal hub. Note the strong compression of the periodic phases embedded in the wide background of chaos (represented in black). (d) Details of the sequence of *odd* shrimps and their legs. (e) Details of the sequence of *even* shrimps and legs. Each individual panel displays the analysis of $2400 \times 2400 = 5.76 \times 10^6$ parameter points. Units of R_1 and R_2 are Ω .

given by the remainder of the integer division of their number of peaks in one period by 17. Multiples of 17 are given the index 17. Of course, the number 17 plays no role, the sequence of colors having been chosen so as to maximize contrast between phase boundaries. Black is used to represent “chaos” (i.e. lack of numerically detectable periodicity). From these figures one sees that the number of peaks contained in one period of $v_2(t)$ increases steadily by 2 after every turn towards the focal hub.

Figure 2 describes in details how the stable oscillations organize themselves and pave with a multitude of colors the control space near to the focal hub. This figure records two important informations, namely (i) how the number of peaks vary along spirals, and (ii) the precise location where the number of peaks changes. *How* they change is discussed below (Fig. 6). Figure 2 shows that the peaks continue to increase by 2 after every turn towards the focal point. From Figs. 2d and e it is possible to recognize several additional secondary spirals sandwiched between every turn of the main spiral. From additional magnifications (not shown here) it is possible to see that there is an apparently unbounded hierarchy of secondary spirals that get thinner and thinner as one approaches more and more the focal hub. In the lower-left quarter of Fig. 2b one sees that the edges, or legs, composing the main spiral

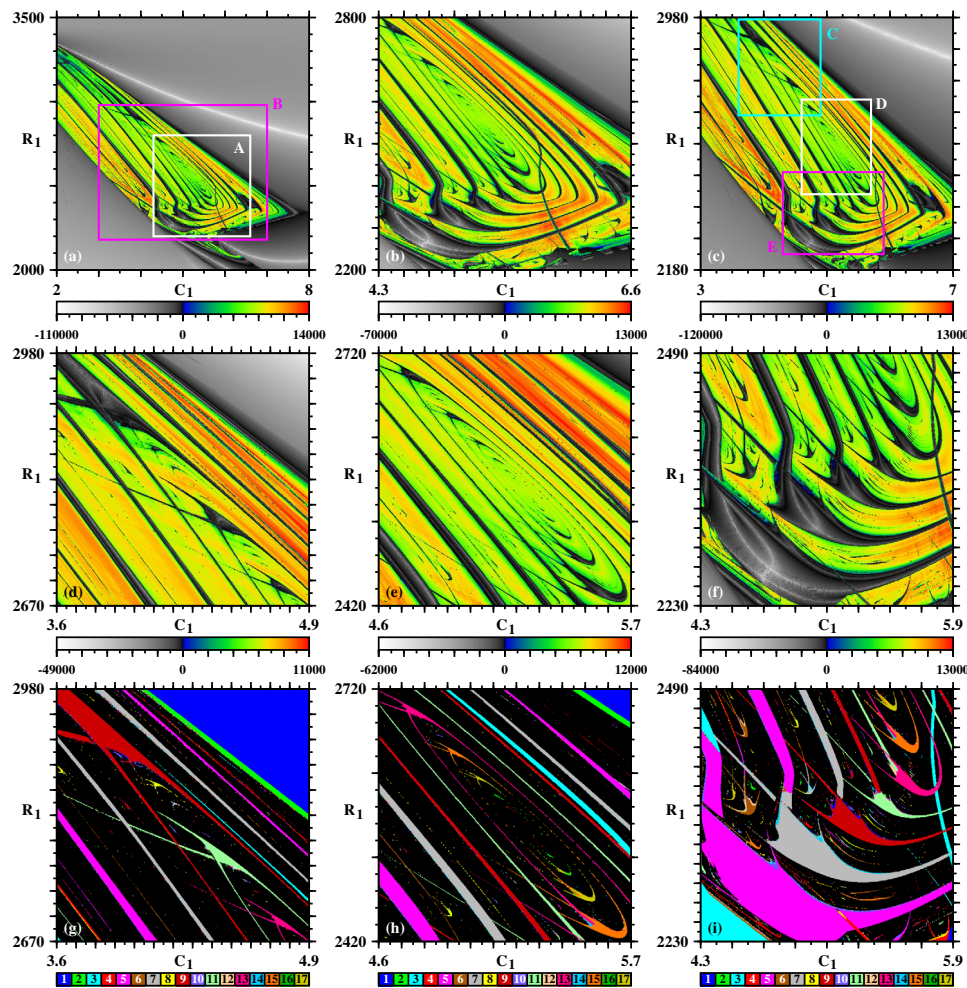


Fig. 3. Two complementary ways of characterizing the stability of the circuit in the $C_1 \times R_1$ control plane: (a)–(f) Lyapunov diagrams, and (g)–(i) isospike diagrams. (a) Global view of the plane, white and pink boxes correspond to the regions plotted in panels (b) and (c). Successive magnifications shown in panels (d)–(f) and (g)–(i) are indicated in the light-blue, white and pink boxes of panel (c). Note the remarkable structural similarity with the structural organization seen in the control plane $R_2 \times R_1$ of Fig. 2. All panels display the number of spikes in one period of $v_2(t)$. Here $L_1 = 12$ mH and $R_2 = 140 \Omega$. Units of R_1 and C_1 are Ω and nF. Each panel shows 600×600 parameter points.

display a clear angularity that, however, becomes smoother and smoother near the hub. We believe that these non-uniformities have to do with the high-dimensionality of the parameter hypersurface defined by the flow. Note that the parameters fixed in Table 1, motivated by experiments, do not produce necessarily optimal sections of this hypersurface, capable of displaying the most symmetric spirals. An optimization of parameters would consume a prohibitively large amount of computer time and, therefore, we have not attempted to do it, selecting for simplicity standard parameter values [6,7]. Apart from the $R_2 \times R_1$ plane, spirals were also found in other planes like, e.g. $C_1 \times C_2$ and $C_1 \times R_1$. Figure 3 shows detailed stability diagrams for this latter control plane. Despite depicting different sections of the parameter space, the

Table 2. Coordinates and the evolution of the number of peaks $p_{v_1}, p_{v_2}, p_{i_1}, p_{i_2}$ of voltages $v_1(t), v_2(t)$ and currents i_1, i_2 when moving towards to the focal point of the spiral. The values of (R_2, R_1) are located near shrimp heads [28, 29] along the spiral. T gives the period of the oscillations.

	$R_2(\Omega)$	$R_1(\Omega)$	T (ms)	p_{v_1}	p_{v_2}	p_{i_1}	p_{i_2}
s_0	92	2137	0.438	5	5	7	3
s_1	5.6	2823	0.504	5	5	7	5
s_2	102	2186	0.631	7	7	9	5
s_3	64	2658	0.696	7	7	9	7
s_4	111	2234	0.809	9	9	11	7
s_5	87	2584	0.888	9	9	11	9
s_6	122	2273	0.991	11	11	13	9
s_7	99.8	2538.5	1.082	11	11	13	11
s_8	130.3	2303.5	1.179	13	13	15	11
s_9	108.5	2508.5	1.274	13	13	15	13
s_{10}	138	2330.0	1.366	15	15	17	13
s_{11}	114	2487	1.464	15	15	17	15
s_{12}	141	2352.5	1.558	17	17	19	15
s_{13}	118.3	2472.5	1.652	17	17	19	17
s_{14}	139.4	2378.5	1.751	19	19	21	17
s_{15}	121	2461.3	1.842	19	19	21	19
s_{16}	136.2	2398	1.944	21	21	23	19
s_{17}	123	2453.4	2.032	21	21	23	21

spirals in Figs. 2 and 3 display a remarkable structural similarity that persists at all levels of magnification shown.

What happens with the periodicity of the oscillatory patterns when one moves along the spiral towards the focal hub? In other words, how do periodic patterns evolve along the spiral? To check this, for the parameter points defined in Table 2 below, we computed the temporal evolution of currents and voltages for a few parameters s_0, s_1, \dots, s_{17} located at the turning points of the spiral, indicated by the dots in Figs. 2a–e. The remarkable outcome of such computations is shown in Fig. 4 which illustrates several things. First, it shows that the widest periodic phases composing the spiral start with oscillations having an *odd* number of spikes. Second, antiperiodic wave patterns evolve continuously when parameters are tuned along the spiral. Third, the waveform displays the same generic form when circling towards the focal hub, while the number of peaks increases steadily by 2 after each turn around the spiral. Four, the temporal evolution of *all periodic voltages and currents with an odd number of spikes displays a clear antiperiodicity* characterized by the relation

$$x\left(t + \frac{T}{2}\right) = -x(t), \quad (4)$$

where x represents any of the four variables v_1, v_2, i_1, i_2 and T is the oscillation period. Of course, Eq. (4) is precisely the signature of the antiperiodic oscillations.

An additional interesting feature of the temporal evolutions in Fig. 4 is that the amplitudes of v_2 recorded at the turning points s_0, s_2, s_4 are smaller than those recorded at s_1, s_3, s_5 . The same is true for i_2 . In other words, not only the period but also the amplitude of the oscillations vary while cycling towards the hub. Note that an antiperiodic function with period T is necessarily a periodic function with period $2T$. Furthermore, note that symmetry forbids antiperiodicity to exist for oscillations with an even number of spikes.

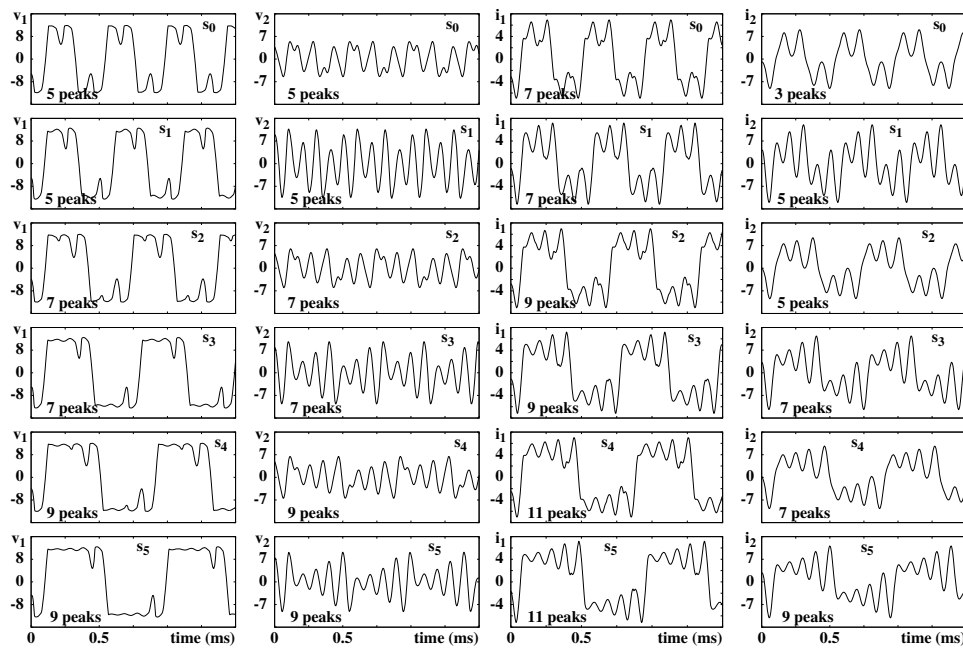


Fig. 4. The first six of the infinite sequence of antiperiodic waveforms observed for v_1, v_2, i_1, i_2 when varying two parameters simultaneously while cycling towards the focal hub. Such parameters are recorded as points $s_0, s_1, s_2, \dots, s_5$ in Table 2. Voltages are measured in V and currents in mA. The time scales shown apply to all panels.

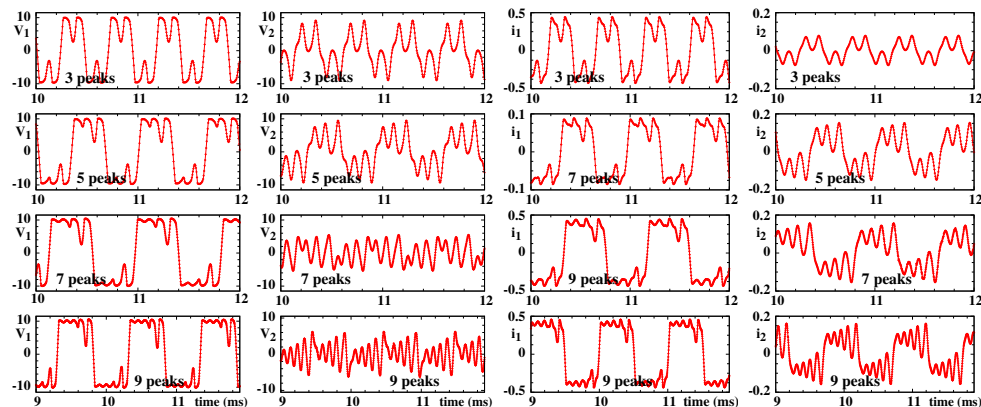


Fig. 5. Experimental waveforms of $v_1(t), v_2(t), i_1(t),$ and $i_2(t)$ when varying R_1 while keeping $R_2 = 118 \Omega$ fixed. The values of R_1 are, from top to bottom $R_1 = 2167 \Omega, R_1 = 2199 \Omega, R_1 = 2291 \Omega, R_1 = 2325 \Omega$. Intensity is given in arbitrary units and voltages in Volts. Other parameter values: $L_1 = 21.4 \text{ mH}, L_2 = 9.8 \text{ mH}, C_1 = 5.86 \text{ nF},$ and $C_2 = 11.8 \text{ nF}$.

Figure 5 depicts experimental results which mimic the unfolding seen in Fig. 4. However, Fig. 5 was obtained while varying just a single control parameter across the spiral and illustrates the fact that variation of a single is enough to discern the rich peak substructure present in the four waveforms. In Fig. 5 one can recognize that the experimental signals corresponding to $i_1(t)$ vary distinctly than the signals in the other three columns. This difference is associate with the fact that the number of peaks in $i_1(t)$ is far more sensitive to noise than the other variables. This is also true

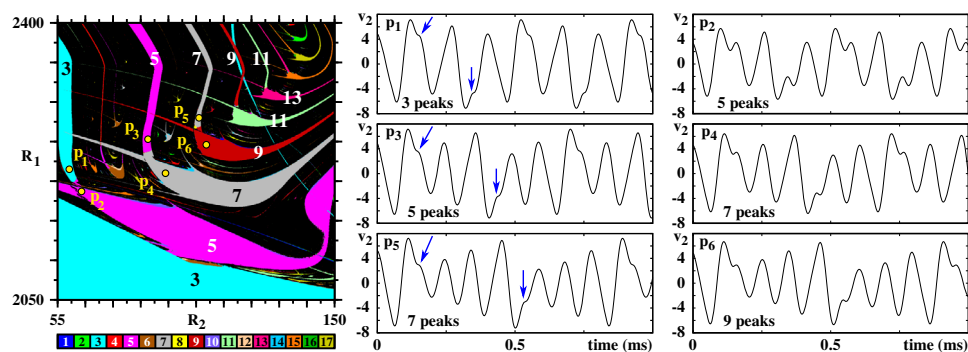


Fig. 6. Changes in the number of spikes occur by local deformations of two peaks, simultaneously. Waveform recorded for the parameters (R_2, R_1) corresponding to the dots in the isospike diagram, $p_1 = (59, 2215)$, $p_2 = (63.2, 2187)$, $p_3 = (86, 2253)$, $p_4 = (92, 2210)$, $p_5 = (103.5, 2280)$, $p_6 = (106, 2246)$, showing the waveform evolution nearby the transitions from 3 to 5, from 5 to 7 and from 7 to 9 peaks. The arrows locate the precursors of new peaks which emerge through waveform deformations (see text). Units of R_1 and R_2 are Ω . The leftmost panel shows 1200×1200 parameter points.

for the numerical simulations of $v_1(t)$ and $i_1(t)$ which, however, due to the higher precision involved, allow peaks to be more accurately computed, in the sense that they are less affected by instrumental imprecisions and can be followed with greater precision. In all figures, the experimental signals corroborate the antiperiodic nature of the oscillations.

From Table 2 one can follow more easily the systematics of the evolution of the number of peaks both for voltages and currents. As it is clear from the Table, the number of peaks of the variables are not always equal although they grow in a regular and predictable way. Comparing the situation between s_0 and s_{17} one sees that, for v_2 , the number of peaks changes from 5 to 21 while the period increases from 0.438 to 2.032 ms, giving $21/5 = 4.2$ and $2.032/0.438 \simeq 4.6$, meaning that the growth of the period is faster than the growth of the number of peaks of the oscillations. The coordinates (R_2, R_1) provide the location of the several $s_0, s_1, s_2, \dots, s_{17}$, some of them marked by dots or labels in the figures above. Such points give the approximate location of the intersection of loci of exponent minima and mimic somewhat the known doubly superstable shrimp heads which are properly defined only for one-dimensional maps [29]. Table 2 also shows the period T of voltages and currents. While the period accumulates to a fixed value when moving towards the focal point, the number of peaks contained in a period seems to grow without bound.

The mechanism responsible for adding peaks along the spiral can be investigated with the help of Fig. 6. In this figure the time evolutions computed immediately before and after changes of the number of peaks for three selected boundaries are represented. The pair of arrows mark the onset of “deformations” of the waveforms that will end up turning into a pair of new peaks. Thus the complexification of the wave patterns arise from deformations analogous to the ones described recently for the prototypical feedback system introduced by Mackey-Glass [13] and for the Lang-Kobayashi model of semiconductor lasers with delayed feedback [14]. These systems, however, do not contain any spirals in their control parameter space and, of course, do not show antiperiodicity. Note that the key for the existence of antiperiodicity in the circuit is the odd number of spikes of the oscillations along the spiral. Furthermore, in order for antiperiodicity to subsist indefinitely on the spirals, we need a pair of wave pattern deformations to occur simultaneously.

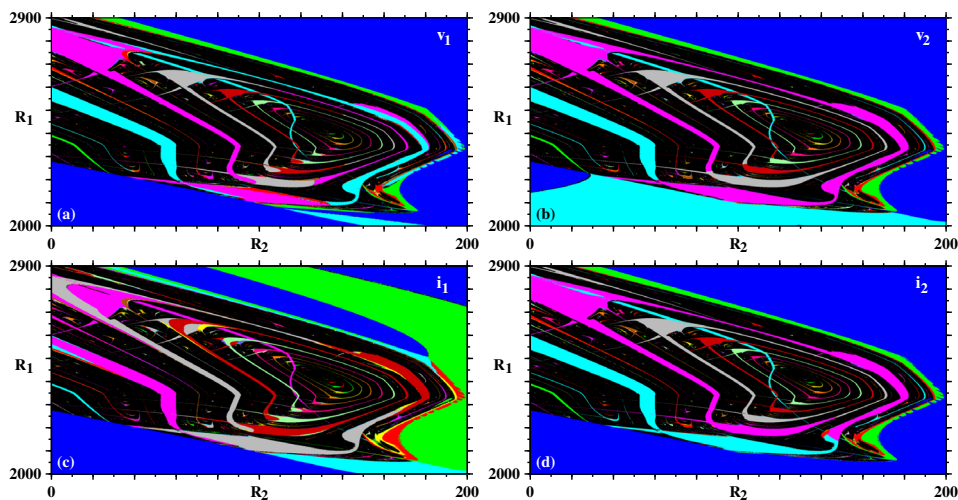


Fig. 7. The size and the boundaries of periodic phases depend on the variable used to count peaks. Isospike diagrams obtained by counting the number of peaks in one period of (a) $v_1(t)$, (b) $v_2(t)$, (c) $i_1(t)$, (d) $i_2(t)$. Table 2 collects the number of peaks for all these variables. The color coding is the same as used in previous figures. Units of R_1 and R_2 are Ω . Each panel records the analysis of $1200 \times 1200 = 1.44 \times 10^6$ parameter points.

So far, our description of the structure of the stability diagrams obtained by counting the number of peaks was based on the study of v_2 , the voltage across the capacitance C_2 in Fig. 1. What happens when one considers the other three variables to count peaks? Do the peaks of all four variables evolve in unison when parameters change? The answer is given in Fig. 7: each variable produces quite different subdivisions of the periodic phases. Every variable yields subdivisions having their own specific idiosyncrasies although the overall trend remains the same. The number of peaks may change after a full turn along the spiral or not. Furthermore, the location where changes occur varies for each variable. An attempt to uncover the systematics behind such changes is too demanding and would only make sense after solving the optimization problem mentioned in the previous paragraph.

As already mentioned, symmetry considerations prevent oscillations with an even number of spikes of being antiperiodic. Thus, although regions of oscillations with an odd number k of spikes display antiperiodicity, the infinite $k \times 2^n$ doubling cascades issuing from them must necessarily display periodic waveforms. Note the peak-doubling cascades that are clearly visible in the lower right corner of the panels in Fig. 7.

4 Conclusions and outlook

We reported a detailed investigation of detectability of spiral stability phases for a nonlinear circuit with two active components. Our results show that spiral phases and regularities are accessible by measuring the dynamics of *any of the four variables of the circuit*. The relative size of the individual stability phases, their boundaries, and the number of peaks of their characteristic oscillations depends on the specific physical quantity used to record them (see Fig. 7). But despite these differences, the global structural organization of the phase diagrams is remarkably invariant for the circuit. Antiperiodic oscillatory wave patterns become more and more complex through a regular spike-adding mechanism involving continuous waveform deformations, not

via period-doubling or other of the familiar mechanisms. Individual stability phases are characterized by specific waveforms (Fig. 4), which evolve continuously along the spiral. While the number of peaks of the periodic oscillations grows indefinitely, their period seems to accumulate to certain values that can be determined if needed.

An interesting open problem is that, while peak-adding cascades (which happen along the spirals) preserve the initial symmetry of the wave forms, in sharp contrast, peak-doubling cascades (happening in the transversal direction) need first to *break the initial symmetry* in order to start to unfold by doubling. Thus, finding the right conditions for adding and doubling cascades of antiperiodic forms seems a nontrivial issue that deserves to be investigated.

JGF was supported by the Post-Doctoral grant SFRH/BPD/43608/2008 from FCT, Portugal. She thanks UFPB for the hospitality. CC and ACM acknowledge support from CSIC and PEDECIBA, Uruguay. JACG thanks support from CNPq, Brazil. This work was supported by the Deutsche Forschungsgemeinschaft through the Cluster of Excellence *Engineering of Advanced Materials*. All bitmaps were computed in the CESUP-UFRGS clusters in Porto Alegre, Brazil.

References

1. D. Urzagasti, D. Laroze, H. Pleiner, Eur. Phys. J. Special Topics **223**, 141 (2014)
2. J.G. Freire, J.A.C. Gallas, Chaos Sol. Frac. **59**, 129 (2014)
3. A. Celestino, C. Manchein, H.A. Albuquerque, M.W. Beims, Commun. Nonlinear Sci. Numer. Simulat. **19**, 139 (2014)
4. A. Hoff, T. Silva, C. Manchein, H.A. Albuquerque, Phys. Lett. A **378**, 171 (2014)
5. D. Laroze, P.G. Siddheshwar, H. Pleiner, Commun. Nonlinear Sci. Numer. Simul. **18**, 2436 (2013)
6. J.G. Freire, C. Cabeza, A. Marti, T. Pöschel, J.A.C. Gallas, Nature Sci. Rep. **3**, 1958 (2013)
7. C. Cabeza, C.A. Briozzo, R. Garcia, J.G. Freire, A.C. Marti, J.A.C. Gallas, Chaos Sol. Frac. **52**, 59 (2013)
8. A. Sack, J.G. Freire, E. Lindberg, T. Pöschel, J.A.C. Gallas, Nature Sci. Rep. **3**, 3350 (2013)
9. W. Façanha, B. Oldeman, L. Glass, Phys. Lett. A **377**, 1264 (2013)
10. E.S. Medeiros, R.O. Medrano, I.L. Caldas, S.L.T. de Souza, Phys. Lett. A **377**, 628 (2013)
11. S.L.T. de Souza, A.A. Lima, I.L. Caldas, R.O. Medrano, Z.O. Guimarães-Filho, Phys. Lett. A **376**, 1290 (2012)
12. L. Gardini, F. Tramontana, S. Banerjee, Math. Comput. Simul. **95**, 137 (2013)
13. L. Junges, J.A.C. Gallas, Phys. Lett. A **376**, 2109 (2012)
14. L. Junges, T. Pöschel, J.A.C. Gallas, Eur. Phys. J. D **67**, 149 (2013)
15. R. Barrio, F. Blesa, S. Serrano, A. Shilnikov, Phys. Rev. E **84**, 035201(R) (2011)
16. R. Barrio, F. Blesa, A. Dena, S. Serrano, Comput. Math. Appl. **62**, 4140 (2011)
17. R. Vitolo, P. Glendinning, J.A.C. Gallas, Phys. Rev. E **84**, 016216 (2011)
18. C. Stegmann, H.A. Albuquerque, R.M. Rubinger, P.C. Rech, Chaos **21**, 033105 (2011)
19. D.F.M. Oliveira, M. Robnik, Phys. Rev. E **83**, 026202 (2011)
20. J.G. Freire, J.A.C. Gallas, Phys. Lett. A **375**, 1097 (2011)
21. J.G. Freire, J.A.C. Gallas, Phys. Chem. Chem. Phys. **13**, 12191 (2011)
22. J.G. Freire, T. Pöschel, J.A.C. Gallas, Europhys. Lett. **100**, 48002 (2012)
23. Z.T. Zhusubaliyev, E. Mosekilde, Physica D **238**, 589 (2009)
24. J.G. Freire, J.A.C. Gallas, Phys. Rev. E **82**, 037202 (2010)
25. A. Celestino, C. Manchein, H.A. Albuquerque, M.W. Beims, Phys. Rev. Lett. **106**, 234101 (2011)
26. C. Bonatto, J.A.C. Gallas, Phys. Rev. Lett. **101**, 054101 (2008)

27. C. Bonatto, J.A.C. Gallas, *Phil. Trans. Royal Soc. London Series A* **366**, 505 (2008)
28. For a survey see J.A.C. Gallas, *Int. J. Bif. Chaos* **20**, 197 (2010), and references therein
29. J.A.C. Gallas, *Physica A* **211**, 57 (1994)
30. E.V. Viana, R.M. Rubinger, H.A. Albuquerque, A.G. de Oliveira, G.M. Ribeiro, *Chaos* **20**, 023110 (2010)
31. D.F.M. Oliveira, E.D. Leonel, *Phys. Lett. A* **376**, 3630 (2012)
32. D.F.M. Oliveira, E.D. Leonel, *New J. Phys.* **13**, 123012 (2011)
33. E.N. Lorenz, *Physica D* **237**, 1689 (2008)